Optimal design of multi-channel microreactor for uniform residence time distribution

Cyril Renault · Stéphane Colin · Stéphane Orieux · Patrick Cognet · Théo Tzédakis

Abstract Multi-channel microreactors can be used for various applications that require chemical or electrochemical reactions in either liquid, gaseous or multi phase. For an optimal control of the chemical reactions, one key parameter for the design of such microreactors is the residence time distribution of the fluid, which should be as uniform as possible in the series of microchannels that make up the core of the reactor. Based on simplifying assumptions, an analytical model is proposed for optimizing the design of the collecting and distributing channels which supply the series of rectangular microchannels of the reactor, in the case of liquid flows. The accuracy of this analytical approach is discussed after comparison with CFD simulations and hybrid analytical-CFD calculations that allow an improved refinement of the meshing in the most complex zones of the flow. The analytical model is then extended to the case of microchannels with other cross-sections (trapezoidal or circular segment) and to gaseous flows, in the continuum and slip flow regimes. In the latter case, the model is based on second-order slip flow boundary conditions, and takes into account the compressibility as well as the rarefaction of the gas flow.

C. Renault · S. Colin (✉) · S. Orieux
Université de Toulouse; INSA, UPS, Mines Albi, ISAE;
ICA (Institut Clément Ader), 135, avenue de Rangueil,
31077 Toulouse, France
e-mail: stephane.colin@insa-toulouse.fr

C. Renault
e-mail: renault.cyril@hotmail.fr

S. Orieux
e-mail: stephane.orieux@insa-toulouse.fr

C. Renault · P. Cognet · T. Tzédakis
Laboratoire de Génie Chimique, Université de Toulouse; INPT,
UPS, 118 Route de Narbonne, F-31062 Toulouse, France
e-mail: patrick.cognet@ensiacet.fr

T. Tzédakis
e-mail: tzedakis@chimie.ups-tlse.fr

C. Renault · P. Cognet · T. Tzédakis
Laboratoire de Génie Chimique, CNRS, 31062 Toulouse, France

1 Introduction

Applications of microfluidic systems are very varied and have been developed for more than two decades (Gravesen et al. 1993; Shoji and Esashi 1994). They are now used for example in aerospace, automotive, military, food and also in a number of medical applications. The recent development of MEMS and microfluidic technologies applied to chemical engineering is due to several advantages among which the increased surface area to volume ratio (Löwe and Ehrfeld 1999) which greatly improves the mass or energy transfer. Thanks to their small dimensions, microreactors exhibit fast response times, which is an advantage for the process control and permits the use of highly reactive and dangerous products (Vlachos 1998). In comparison with macroscopic reactors, microreactors allow a better management of effective heat, facilitating isothermal operation or coupling of endothermic and exothermic reactions (Peterson 1999). All these features associated to original designs can allow reducing the number of reaction steps. In addition, miniaturization should help to optimize selectivity, reduce energy consumption and lower production costs. Thus, the current trend is to develop smaller, cheaper and more efficient devices by optimizing safety and reaction control while minimizing the environmental impact (Commenge et al. 2005).

There are some counterparts, however, to the use of microreactors. Reduction of dimensions may lead to

significant modifications of both flow hydrodynamics and convective heat transfer, especially in the case of gases, for which rarefaction of the flow induces local thermodynamic disequilibrium. Another restriction is due to the small volumes that limit the possibilities of industrial production. To overcome this drawback, the use of several parallel microchannels is necessary but this solution could exhibit a poor uniformity in the fluid distribution between them. Recently, Ziogas et al. (2009) have summarized the advantages and disadvantages of the use of microreactors compared with conventional reactors applied to electrochemistry.

An example of typical microreactor made of a series of parallel microchannels is shown in Fig. 1. The three main parts of this basic cell are the distributing channel, the network of parallel reaction microchannels and the collecting channel. The arrows point out the possible locations of the flow inlet and outlet. Applications for such a microreactor design are varied. A simple microreactor can for example be used in synthesis of organic compounds and in catalytic treatment of gaseous effluents contaminated by volatile organic compounds (VOCs). An electrochemical microreactor can be designed for electro synthesis of "probes" molecules devoted to medical imaging for tumor detection, using two similar gold- or platinum-coated units facing each other and separated by an ion-exchanger membrane.

In such a microreactor, the control of the residence time of the fluid is crucial for an efficient operation. The objective is to obtain a uniform distribution of the flowrate between all microchannels. A complete CFD simulation of complex microreactor geometries generally requires, however, important computational resources (Commenge et al. 2002; Saber et al. 2009). Delsman et al. (2004) proposed an optimization of the flow distribution in a microstructured plate composed with 19 rectangular microchannels,

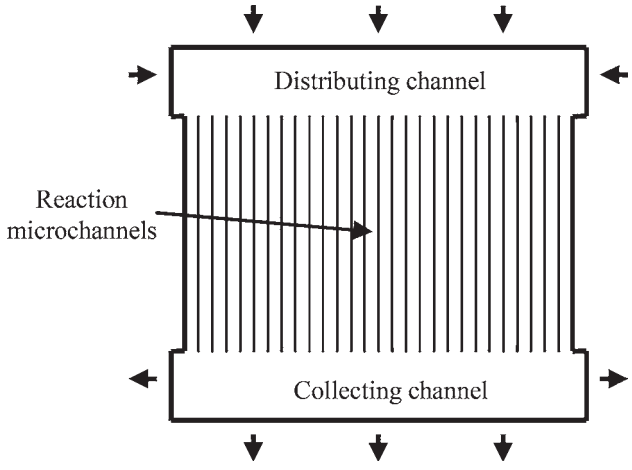

Fig. 1 Example of microreactor based on a network of parallel microchannels

considering nine plate designs with different distributing and collecting channels and locations of the inlet and outlet sections, under various flowrate conditions. The authors used a three-dimensional CFD model with an artificial viscosity in the channel region which reduced the computational time by a factor 7. The simulations showed that doubling the cross-sectional area of the distributing and collecting channels improved the even distribution of the flow. The same trend was observed by doubling the length of the microchannels. Finally, the best geometry found consisted in inlets and outlets sections parallel to the microchannels cross-sections, with asymmetrical distributing and collecting channels. With this optimal design, the relative standard deviation of the flow distribution was reduced from 19 to 3%. Jang et al. (2010) developed an original program combining a simplified conjugate-gradient method called SCGM (Chen and Cheng 2002) with CFD calculation by the CFD-ACE + commercial code in order to optimize the width of distributing and collecting channels. Their goal was to increase the methanol conversion for hydrogen production in fuel cells. They compared three different geometries with different inlet and outlet locations and found an optimized solution for these three cases which required an increase in the pressure drop. They also showed that this optimization led to an improvement of the methanol conversion ratio from 72.7 to 99.9%.

In order to rapidly optimize the design of multi-channel microreactors, it is necessary to develop calculation methods less expensive in terms of memory and computation time. Commenge et al. (2002) proposed an approximate model in order to evaluate the pressure drop and flow distribution through microchannels, focusing on the influence of the length and width of the reaction microchannels and the angle of the tapered distributing and collecting channels. CFD calculations were used to validate this analytical model. Saber et al. (2009) analyzed the hydrodynamics of multi-scale channel networks under isothermal and laminar conditions, using a linear pressure drop model. The main technique used to improve the uniformity of the residence time distribution was to decrease the pressure drop through the distributing and collecting channels in comparison to the pressure drop through the microchannels. This objective was achieved increasing the distributing over microchannel hydraulic diameter ratio and decreasing the distributing over microchannel length ratio. More recently, Saber et al. (2010) investigated the performances of their previous multi-scale channel network, focusing on the selectivity of consecutive catalytic reactions. The authors demonstrated the large influence of the flow maldistribution on the selectivity, which reduces the efficiency of the considered reaction. Cho et al. (2010) studied the thermal and hydrodynamic behaviour of microchannel heat sinks with a design similar to the one shown in Fig. 1. They investigated

the effect of non-uniform heat flux for three different non-uniform heat flux conditions, using a tri-diagonal matrix algorithm (TDMA) for the calculation of mass flow distribution. The influence of the shape of the distributing and collecting channels on the two-phase flow distribution in the rectangular microchannels was also analysed. It was concluded that a more even flow distribution is achieved when the cross-sectional area of the distributing and collecting channel are larger, compared with the cross-sectional area of the microchannels.

Whatever its design, the optimisation of a microreactor requires an accurate modelling of the hydrodynamics in the distributing and collecting channels, as well as in the microchannels, which have the smallest hydraulic diameters of the reactor. Due to the low values of the Reynolds numbers, the analytical modelling of liquid flows in long microchannels is easy. For fully developed laminar and isothermal flows of Newtonian liquids, the Poiseuille number is a constant that only depends on the shape of the channel cross-section. The early experimental studies published twenty years ago, however, showed deviations from the theory and pointed out contradictory results (Morini 2004), but the most recent papers have shown that these deviations were mainly due to experimental uncertainties, particularly the uncertainties on the dimensions of the channel cross-section. Thus, conventional theory has now proved to be accurate for predicting liquid flowrates in microchannels, as soon as the hydraulic diameter is of the order of one micrometer or higher.

On the other hand, reducing dimensions or decreasing pressure leads to rarefaction effects, in addition to compressibility effects, for flows of gases in microchannels (Colin 2005). These rarefaction effects appear as soon as the mean free path of the molecules is no longer negligible compared with the hydraulic diameter of the microchannel. For such rarefied flows, the classic Poiseuille model is no longer valid, and other models should be used, according to the rarefaction level, which is quantified by the Knudsen number $Kn = \lambda/L$, ratio of the mean free path of the molecules λ over a characteristic length L such as the hydraulic diameter. In microsystems, it is frequent that $10^{-3} \leq Kn \leq 10^{-1}$; in that case, the regime is the so-called slip flow regime and the Navier–Stokes equations remain applicable, provided a velocity slip and a temperature jump at the walls, due to a local thermodynamic disequilibrium, are taken into account. Semi-analytical models are still available in this regime, even when 3-D effects should be taken into account, as it is the case for rectangular cross-sections (Aubert and Colin 2001).

The objective of the present paper is to propose a simple model for the rapid optimisation of a multi-channel microreactor, in terms of uniform residence time distribution. Following the description of a multi-channel microreactor in Sect. 2, an analytical model is developed in Sect. 3, which allows a rapid calculation of the flow distribution of liquids in the rectangular microchannels as a function of the geometrical parameters. The efficiency of this approximate model is validated by CFD simulations and a hybrid model combining these two approaches is proposed. This intermediate approach allows the utilisation of simple analytical equations in the long straight microchannels, combined with accurate CFD calculations for the other parts of the microreactor which require more complex 3D simulations. The analytical model is extended in Sect. 4 to the case of microchannels with various cross sections. In silicon substrates, rectangular cross-sections can be etched by deep reactive ion etching (DRIE) whereas trapezoidal cross-sections are obtained by wet chemical etching. In metallic substrates, circular segment sections can be obtained by precision micro milling, embossing, isotropic wet chemical etching (Madou 2002) or micro electro discharge machining (μEDM) techniques. Finally, it is shown that the analytical model can also be extended to the case of gas flows in the continuum and slip flow regimes. From these models, it is demonstrated that the microreactor can exhibit a uniform residence time distribution in the microchannels, by simply modifying one geometrical parameter of the distributing and collecting channels.

2 Microreactor geometry

2.1 Overall view

A schematic view of a microreactor, here designed for electrochemical synthesis of molecules, is shown in Fig. 2. It is composed of two symmetrical units facing each other. A copper heat exchanger (E) insures the extraction of heat generated by the chemical reaction, the coolant fluid flowing through the cavity with internal zigzag from inlet (E_I) to outlet (E_O). A thick plate of platinum (P), or a silicon plate with a platinum deposit, is welded to the heat exchanger side. Microchannels are etched in this plate which plays the role of an electrode. The chemical solution flows through these microchannels. Two platinum tubes are inserted through the copper block and the bottom face of the platinum layer allowing the entrance (T_I) and exit (T_O) of the chemical fluid. Both electrodes (anode and cathode) are separated by an ion-exchanger membrane (M).

2.2 Electrodes

Figure 3 details the initial geometry of the electrodes, with the distributing channel, the reaction microchannels and the

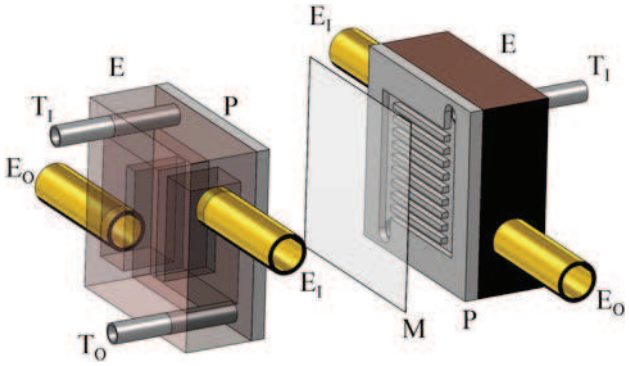

Fig. 2 Schematic view of the electrochemical microreactor

collecting channel. Table 1 provides typical values of the various parameters defining non-optimized electrode geometry, in the case of 10 parallel microchannels with rectangular cross-sections. These values are used in Sect. 3.4 for illustrating the calculation of an optimal design.

2.3 Optimisation strategy

The aim of the optimization is to design the distributing and collecting channels in order to obtain the most possible uniform residence time distribution among all microchannels. For simplifying the fabrication process, the depth of the distributing and collecting channels, as well as the depth of the reactor microchannels is kept uniform and constant ($d = 50\,\mu$m). It is demonstrated in Sects. 3 and 4 that a uniform residence time distribution can be achieved optimizing a single parameter: the angle θ of the tapered distributing and collecting channels, initially equal to zero (see Fig. 4).

3 Optimisation for liquid flows and rectangular microchannels

3.1 Analytical model

The following analytical model is very simple to implement and provides flowrate and pressure drop distributions in a few seconds, assuming a laminar regime in the entire microreactor. The distributing and collecting channels are considered as a series of short segments with rectangular cross-sections (Fig. 5). The unknowns are the inlet and outlet pressures P_{in} and P_{out} as well as the volume flow rates Q_j—or the mass flowrate $\dot{M}_j$—for each microchannel j.

Figure 5 illustrates the simplifying assumptions in the case of 10 reaction microchannels. The pressures calculated at the downstream section of each segment of the distributing channel are reported to the inlet of the corresponding microchannel, while the pressures at the outlet of each microchannel are reported to the upstream section of

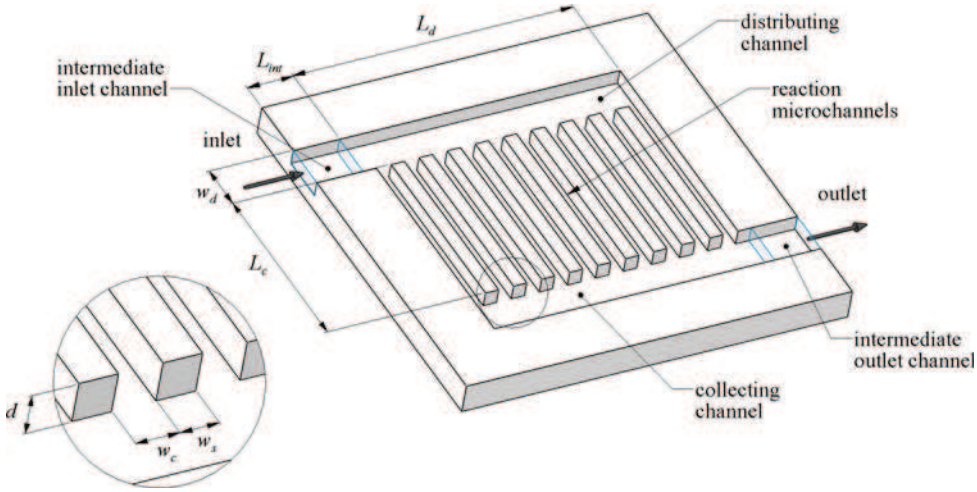

Fig. 3 Diagram of the initial electrode before optimization

Table 1 Example of geometrical parameters of the initial electrode before optimization

	Reaction microchannels	Distributing/collecting channels
Number of channels	10	1/1
Length	L_c = 5 mm	L_d = 5 mm
Depth	d = 50 µm	d = 50 µm
Width	w_c = 250 µm	w_d = 1 mm
Width of walls between channels	w_s = 250 µm	

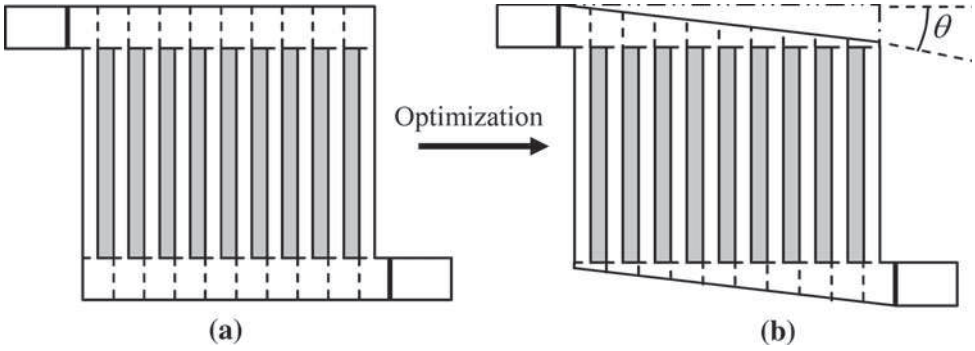

Fig. 4 Initial (**a**) and optimal (**b**) geometries of the electrode

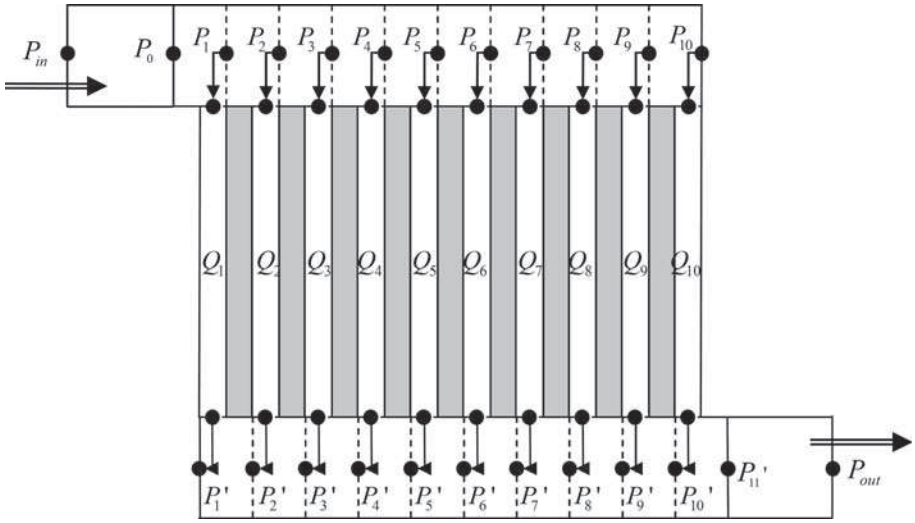

Fig. 5 Diagram of an electrode and its associated network of microchannels (case of 10 reaction microchannels)

the corresponding segment in the collecting channel. The pressure drop ΔP through any segment of the collecting and distributing channels or through the reaction microchannels is related to the corresponding volume flowrate Q or mass flowrate $\dot{M}$ with the Poiseuille number

$$Po = \frac{SD_h^2 \Delta P}{2\mu Q\ L} = \frac{\rho SD_h^2 \Delta P}{2\mu \dot{M}\ L}, \tag{1}$$

whose value only depends on the aspect ratio of the rectangular cross-section. In Eq. 1, S is the cross-section area, D_h is the hydraulic diameter, μ and ρ are the dynamic viscosity and the density of the fluid, respectively, and L is the length of the considered channel segment or microchannel. The Poiseuille number for a rectangular cross-section can be calculated from the polynomial (Shah and London 1978)

$$Po_R = 24\Big[1 - 1.3553r_R^* + 1.9467r_R^{*^2} - 1.7012r_R^{*^3} + 0.9564r_R^{*^4} - 0.2537r_R^{*^5}\Big] \tag{2}$$

where $0 < r_R^* \leq 1$ is the aspect ratio of the rectangular section defined by $r_R^* = d/w_c$. In the general case of a microreactor with n microchannels, the problem reduces to a set of $3n + 2$ equations of type (1), $n + 1$ for the distributing channel, n for the reaction microchannels and $n + 1$ for the collecting channel (see Figs. 3 and 5). The $3n + 2$ unknowns are P_j and P_j' with $j \in [0; n]$ and $\dot{M}_i$ with $i \in [1; n]$. Each quantity

$$R_{h,\alpha-\beta} = \frac{2\mu LPo}{\rho SD_h^2} \tag{3}$$

represents the hydraulic resistance of the considered channel segment or microchannel, with an inlet pressure P_α and an outlet pressure P_β, and it is calculated with Eq. 2 which gives the value of Po. The system of equations is then written in the matrix form

$$\mathbf{C} = \mathbf{AB}, \tag{4}$$

where $\mathbf{B}$ contains the unknowns, $\mathbf{C}$ is function of the inlet pressure P_{in} and outlet pressure P_{out} of the microreactor and $\mathbf{A}$ is function of the various hydraulic resistances (3) previously calculated. For example, in the simple case of a microreactor with only two microchannels, Eq. 4 reads:

$$\begin{vmatrix} P_{in} \\ 0 \\ 0 \\ 0 \\ 0 \\ 0 \\ 0 \\ P_{out} \end{vmatrix} = \begin{vmatrix} +1 & 0 & 0 & 0 & 0 & 0 & R_{h,in-0} & R_{h,in-0} \\ -1 & +1 & 0 & 0 & 0 & 0 & R_{h,0-1} & R_{h,0-1} \\ 0 & -1 & +1 & 0 & 0 & 0 & 0 & R_{h,1-2} \\ 0 & -1 & 0 & +1 & 0 & 0 & R_{h,1-1'} & 0 \\ 0 & 0 & -1 & 0 & +1 & 0 & 0 & R_{h,2-2'} \\ 0 & 0 & 0 & -1 & +1 & 0 & R_{h,1'-2'} & 0 \\ 0 & 0 & 0 & 0 & -1 & +1 & R_{h,2'-3'} & R_{h,2'-3'} \\ 0 & 0 & 0 & 0 & 0 & +1 & -R_{h,3'-out} & -R_{h,3'-out} \end{vmatrix} \times \begin{vmatrix} P_0 \\ P_1 \\ P_2 \\ P'_1 \\ P'_2 \\ P'_3 \\ \dot{M}_1 \\ \dot{M}_2 \end{vmatrix}.$$

The solution of the problem is given by

$$\mathbf{B} = \mathbf{A}^{-1}\mathbf{C}, \tag{5}$$

where $\mathbf{A}^{-1}$ is the inverse of $\mathbf{A}$, which can be easily calculated using Matlab software.

3.2 CFD simulation

The accuracy of the analytical model is analyzed by comparison with numerical simulations obtained with the commercial CFD code Fluent. Different meshes are generated and tested. Only one half of the real domain is meshed, as the plane located at the half-depth of the channels is a plane of symmetry.

For the first mesh (A-1), the whole simulated domain (distributing and collecting channels as well as and reaction microchannels) is meshed with a uniform meshing density and 22,400 cells in the main plane (Fig. 6). The second mesh (A-2) is uniformly refined in both directions of the main plane, leading to a number of cells 4 times higher than in the previous case. The third mesh (A-3) is based on the first one with a refinement in the regions of the microchannels inlets and outlets (see Fig. 6). For these three meshes, the influence of the number of cells in the direction of the depth is also checked: 5, 10 and 20 cells in the half-depth of the microreactor are tested (see Table 2). As an example, the case A-2-10 corresponds to the mesh A-2 in the main plane with 10 cells in the half-depth, and the total number of cells for this case is 896,000.

Table 2 Total number of cells in all cases simulated by CFD

Number of cells in depth	5	10	20
Mesh in the main plane			
A-1	112,000	224,000	448,000
A-2	448,000	896,000	1,792,000
A-3	186,970	373,940	747,880
B-1	72,000	144,000	288,000
B-2	84,000	168,000	336,000
B-3	336,000	672,000	1,344,000

All simulations are performed assuming a laminar incompressible and isothermal flow. A pressure-based solver is used with a second-order discretization scheme.

3.3 Hybrid approach

The idea is here to combine the two previous analytical and numerical approaches. As the Poiseuille number in long microchannels is accurately modeled in laminar regime by Eq. 1, it is possible to make CFD simulations only in the collecting and distributing channels and to use analytical modeling for the flow in the microchannels. Equation 1 is implemented via User Defined Functions that allow to link for each microchannel j the inlet pressure P_j, the outlet pressure P'_j and the flowrate Q_j. As the microchannels are not meshed, it is possible to increase the number of cells for the meshing of the distributing and collecting channels, with the same computational effort. Three different meshes

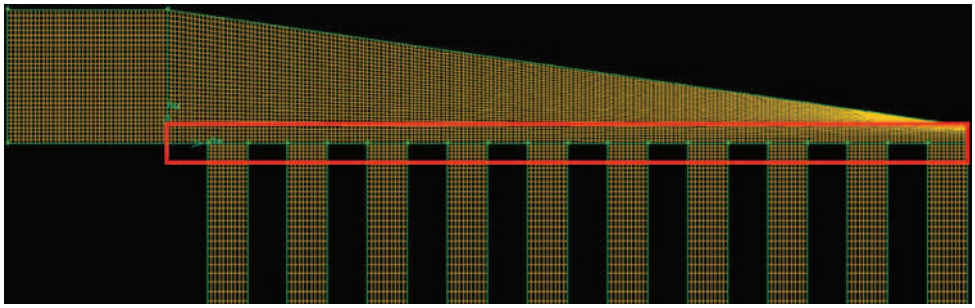

Fig. 6 Detail of the mesh (A-1) in the main plane. The *red rectangle* shows the region refined in mesh A-3

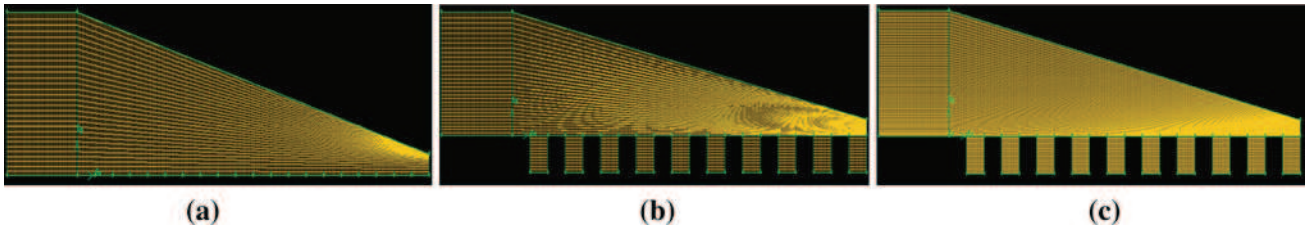

Fig. 7 Meshes of the distributing channel for the hybrid approach; **a** mesh B-1; **b** mesh B-2 and **c** mesh B-3

are used for this hybrid approach (Fig. 7). In case B-1, only the distributing and collecting channels are meshed and in cases B-2 and B-3, the entrance and exit of the microchannels are also meshed to take into account extremity effects, where the flow is not fully developed. Figure 7 shows the mesh in the main plane and Table 2 provides the number of cells for each case. For the three cases, the influence of the number of cells in the depth has also been tested.

3.4 Results and discussion

3.4.1 Analytical optimisation

The analytical model is used to optimise the distributing and collecting channels angle θ in order to obtain the same flowrate in each microchannel. The solution is illustrated for the case of a microreactor with 10 parallel microchannels, the dimensions of which are given in Table 1. The inlet pressure is 10 kPa higher than the outlet pressure. The Reynolds numbers in the microchannels are then in the range $10^{-1} - 10^{1}$. The initial configuration with straight distributing and collecting channels ($\theta = 0$) leads to high deviations between flowrates in the different microchannels: the flowrate in microchannels 1 and 10 is about 50% higher than in the central microchannels 5 and 6 (Fig. 8). After optimisation, the deviation is found negligible for an angle $\theta_R = 10.46°$.

3.4.2 CFD simulations

Table 3 shows the results of the numerical simulation for meshes A-1, A-2 and A-3. The mass flowrate deviation between the data obtained by CFD simulation and the results of the analytical model are provided.

The average deviation between analytical and numerical calculations is of the order of 5%, but larger deviations are experienced for side microchannels 1 and 10, and lower for central microchannels 3–8. By construction of the model, the analytical solution exhibits symmetry: the flowrate in microchannel j is the same as in microchannel $n - j$. On the other hand, the local hydrodynamics at the bifurcations is properly taken into account by the CFD simulation and consequently the symmetry is no longer observed for the numerical solution, but the deviation to this symmetry remains moderate. It should also be noted that an increase in mesh refinement leads to a decrease in the deviation between analytical and numerical data. Due to too many cells in the most refined meshes A-2-10, A-2-20 and A-3-20, numerical simulations in these cases experienced convergence issues. For this reason, the hybrid approach is an interesting alternative: as the microchannels are not

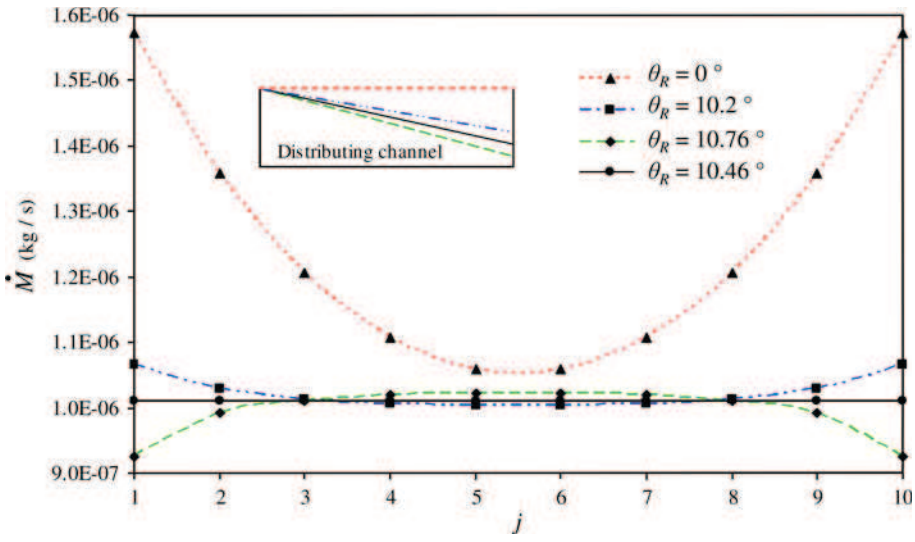

Fig. 8 Flowrate distribution in a 10-microchannel microreactor for the initial layout ($\theta = 0$) and the optimal layout ($\theta = 10.46°$). Flow of water; analytical calculations

Table 3 Deviation (%) on mass flowrate obtained for each microchannel between CFD simulations and analytical model, for various meshes

Channel number j	Analytical solution $\dot{M}(\mathrm{kg\ s^{-1}})$	Deviation between analytical and hybrid data (%)					
		A-1-5	A-1-10	A-1-20	A-2-5	A-3-5	A-3-10
1	1.01×10^{-6}	11.84	9.98	9.54	11.41	11.8	10.2
2	1.01×10^{-6}	6.81	5.01	4.6	6.25	6.73	5.09
3	1.01×10^{-6}	5.03	3.25	2.85	4.36	4.93	3.26
4	1.01×10^{-6}	4.27	2.5	2.11	3.53	4.16	2.47
5	1.01×10^{-6}	4.04	2.26	1.88	3.25	3.91	2.2
6	1.01×10^{-6}	4.17	2.39	2.01	3.37	4.03	2.32
7	1.01×10^{-6}	4.71	2.92	2.53	3.9	4.56	2.84
8	1.01×10^{-6}	5.84	4.03	3.63	5.05	5.67	3.96
9	1.01×10^{-6}	8.2	6.34	5.93	7.43	8	6.29
10	1.01×10^{-6}	14.09	12.15	11.71	13.3	13.85	12.14
Average deviation (%)		6.9	5.08	4.68	6.19	6.76	5.08

meshed, it is possible to use more refined meshes in the distributing and collecting channels with the same computational effort.

3.4.3 Hybrid calculations

The results obtained by the hybrid model are summarised in Table 4.

Similar deviations are observed between hybrid simulation and analytical data, than between CFD and analytical data. It is assumed that the simulations for cases B-2-20 and B-3-10 are the most accurate, as they correspond to the most refined meshes. In these cases, the average deviation with the analytical results is less than 4%, but as previously, larger deviations, between 9 and 13%, are observed in side microchannels 1 and 10. This phenomenon can be explained by a more detailed analysis of the flow in the distributing and collecting channels. In the analytical model, it is assumed that pressure is uniform in both inlet and outlet sections of each segment of distributing and collecting channels. Moreover, it is also assumed that these pressures are the same as the pressures at the inlet or outlet sections of the corresponding microchannels (see Fig. 5).

As illustrated in Fig. 9, which shows the actual contours of pressure obtained by the hybrid simulation with mesh B-3-5, this simplifying assumption is rather accurate at the inlet of the first microchannels and at the outlet of the last microchannels (see for example the zoom on pressure contours P_1 and P'_7). On the other hand, it is less accurate when the distributing and collecting channels are more narrow (see the zoom on pressure contours P_9 and P'_2). Figure 9 also underlines the necessity to simulate by CFD the entrance and exit regions of the microchannels, up to a section in which the pressure is uniform. This is necessary for the validity of Eq. 1 involved in the User Defined Functions.

Table 4 Deviation (%) on mass flowrate obtained for each microchannel between hybrid simulations and analytical model, for various meshes

Channel number j	Analytical solution $\dot{M}(\mathrm{kg\ s^{-1}})$	Deviation between analytical and hybrid data (%)							
		B-1-5	B-1-10	B-1-30	B-2-5	B-2-10	B-2-20	B-3-5	B-3-10
1	1.01×10^{-6}	11.62	10.26	9.93	10.4	8.98	8.63	10.4	9.02
2	1.01×10^{-6}	6.05	4.67	4.34	5.62	4.19	3.85	5.43	4.03
3	1.01×10^{-6}	3.99	2.6	2.29	3.92	2.48	2.16	3.61	2.2
4	1.01×10^{-6}	3.11	1.72	1.41	3.2	1.75	1.43	2.82	1.4
5	1.01×10^{-6}	2.82	1.41	1.1	2.97	1.52	1.2	2.55	1.12
6	1.01×10^{-6}	2.94	1.53	1.22	3.11	1.64	1.33	2.66	1.22
7	1.01×10^{-6}	3.5	2.07	1.76	3.54	2.15	1.83	3.11	1.73
8	1.01×10^{-6}	4.69	3.24	2.93	4.64	3.21	2.89	4.23	2.82
9	1.01×10^{-6}	7.16	5.67	5.35	6.87	5.43	5.09	6.5	5.09
10	1.01×10^{-6}	12.69	11.62	11.3	12.77	11.32	10.97	12.56	11.14
Average deviation (%)		5.86	4.48	4.16	5.7	4.27	3.94	5.39	3.98

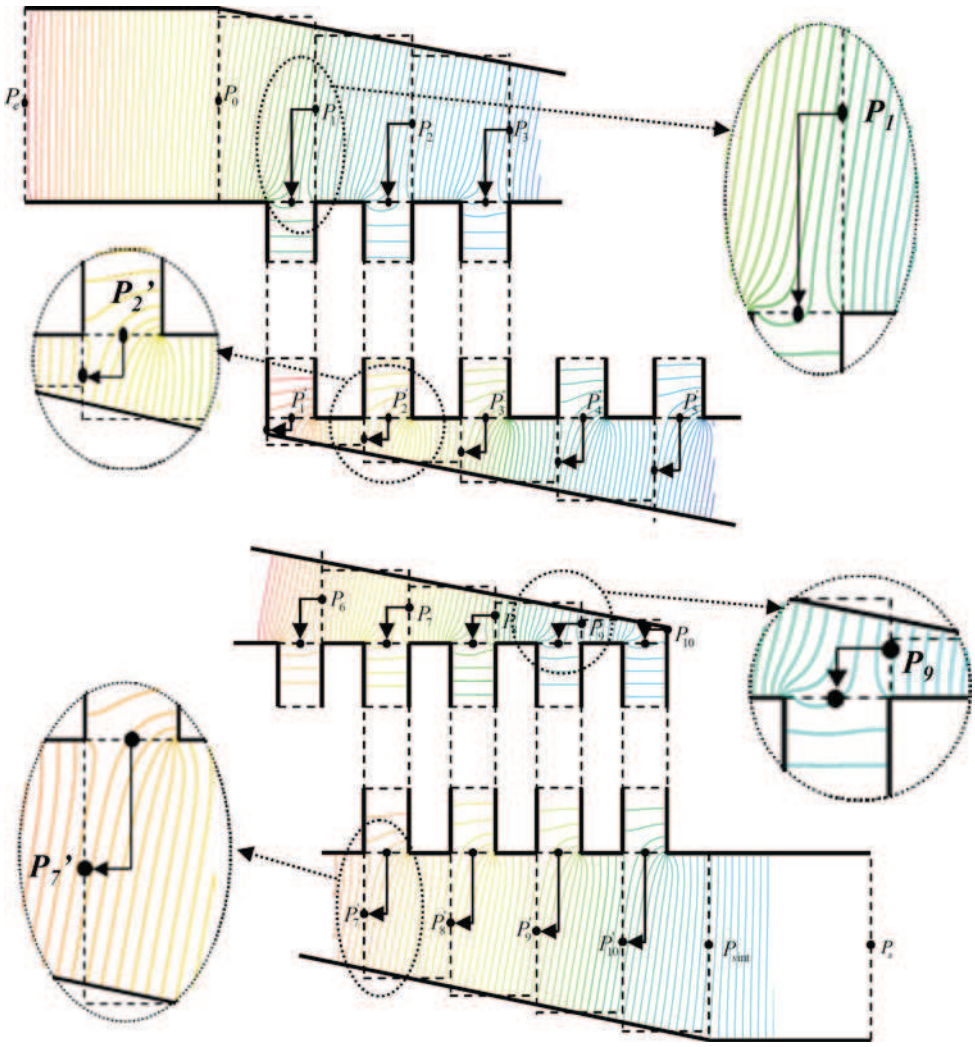

Fig. 9 Iso-contours of pressure obtained by the hybrid simulation with mesh B-3-5

3.5 Optimization with respect to the number of microchannels

The previous optimization has been done for 10 reaction microchannels with an aspect ratio $r_R^* = 0.2$. In this section, the influence of the number n of microchannels on the value of the optimal angle θ is investigated for different aspect ratios ranging from 0.1 to 1. The optimization is based on the previous analytical model; the depth d of the etching is kept equal to 50 μm and the microchannels width w_c is varied in order to analyze various aspect ratios. The length L_c of the microchannels is equal to the length L_d of the distributing and collecting channels, and the width w_s of the walls between two consecutives microchannels is equal to the microchannels width: $L_c = L_d = 2nw_s = 2nw_c$. Figure 10 gives the values of the optimal angle θ_R as a function of n for various aspect ratios r_R^* in a logarithmic scale. It is observed that whatever the aspect ratio, $\theta_R(n)$ exhibits a quasi linear behavior in a logarithmic scale. These curves can be accurately fitted by the general equation

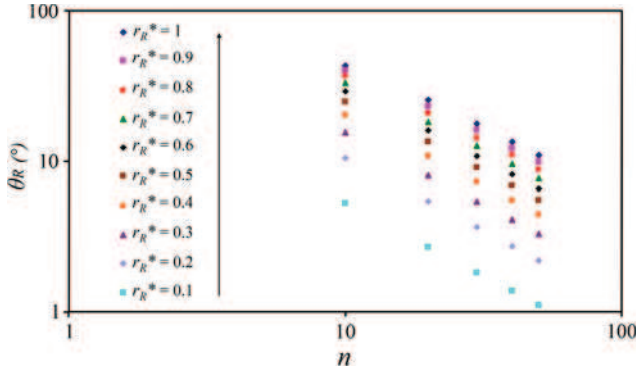

Fig.10 Optimal angle θ_R versus number n of microchannels for various aspect ratios r_R^* in the case of microchannels with rectangular cross-section

$$\theta_R = A_R n^{-B_R} \tag{6}$$

were coefficients A_R and B_R can be expressed as:

$$A_R = 6.4309 + 575.55 r_R^* - 258.71 r_R^{*2} \tag{7}$$

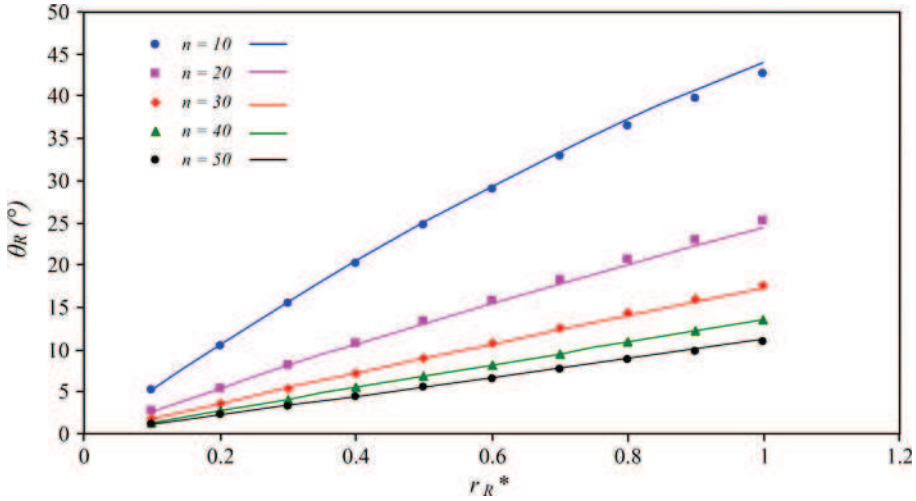

Fig. 11 Optimal angle θ_R versus aspect ratio r_R^* for various numbers n of microchannels, in the case of microchannels with rectangular cross-section.Values calculated by the analytical model (*symbols*) compared with data from Eq. 6 (*solid lines*)

and

$$B_R = 0.9801 - 0.0425 r_R^* - 0.0888 r_R^{*^2}. \quad (8)$$

Figure 11 shows the dependence of the optimal angle θ_R as a function of the aspect ratio r_R^* for a number n of rectangular microchannels ranging from 10 to 50. The symbols represent the optimal angle calculated with the analytical model and the curves are drawn from Eq. 6 associated with Eqs. 7–8. The values obtained by Eq. 6 are in close agreement with the data calculated from the analytical solution (5), with a maximal deviation of less than 3.5% in the case of 20 microchannels and for an aspect ratio $r_R^* = 1$ which corresponds to microchannels with a square cross-section. Equation 6 allows a rapid evaluation of the optimal angle once the number of microchannels and their aspect ratio have been chosen.

4 Extension to other microchannels cross-sections and to gas flow

4.1 Other microchannels cross-sections

The previous analytical model was written for optimizing microreactors with rectangular microchannels. Rectangular cross-sections can for example be obtained by deep reactive ion etching in silicon wafers, or by precision micro-milling in metallic plates, but other cross-sections can also be encountered. For example, trapezoidal cross-sections are obtained by anisotropic wet chemical etching of silicon. In metallic substrates, circular segment sections can be made by precision micro milling, embossing, isotropic wet chemical etching with etchant solution agitation (Madou 2002) or micro electro discharge machining (μEDM) techniques. For that reason, the previous analytical model is extended in this section to the case of microchannels with trapezoidal and circular segment cross-sections (Fig. 12).

For microchannels with trapezoidal cross-section etched in {100} oriented silicon wafers, the etching angle β is equal to 54.74° (Fig. 12b). The trapezoidal cross-section is defined by its depth d, its upper width w_c and its lower width w_c'.

The circular segment cross-sections are defined by their width w_c and their depth d (Fig. 12c). For these three kinds of sections, the aspect ratio is defined by

$$r^* = \frac{d}{w_c}. \quad (9)$$

In the text, the rectangular, trapezoidal and circular segment sections are denoted by the subscripts R, T and C, respectively. In the case of rectangular section, $0 < r_R^* < \infty$. On the other hand, $0 < r_T^* \leq 0.707$ for the trapezoidal

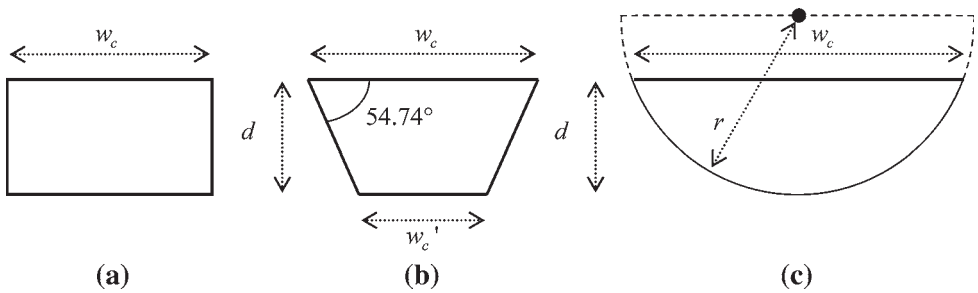

Fig. 12 Rectangular (**a**), trapezoidal (**b**) and circular segment (**c**) cross-sections

section with a limit $r_T^* = 0.707$ corresponding to a triangular section. As for the circular segment section, $0 < r_C^* \leq 0.5$ with a limit $r_C^* = 0.5$ corresponding to a semi-circular section. In the following analysis, the depth is kept equal to 50 µm and $L_c = L_d = 2nw_s = 2nw_c$ for all considered sections.

4.1.1 Trapezoidal cross-section

The Poiseuille number depends on the aspect ratio r_T^* and is estimated by the equation

$$Po_T = 24.320 - 46.877\, r_T^* + 67.533\, r_T^{*2} - 32.339\, r_T^{*3} \tag{10}$$

fitted from the numerical calculation provided in (Morini et al. 2004) (see Fig. 13). The optimal angle is deduced by the analytical solution (5) associated with Eq. 3, in which Po is given by Eq. 2 for the rectangular channel segments

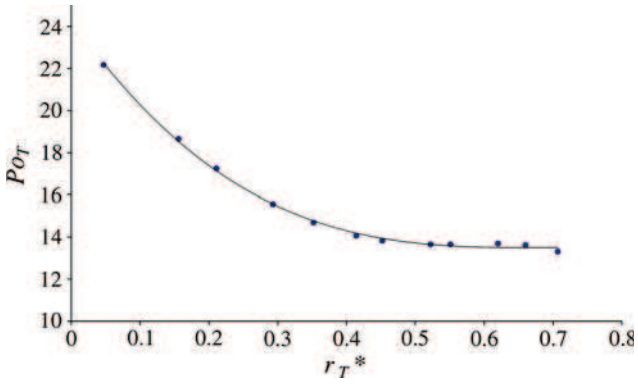

Fig. 13 Poiseuille number versus aspect ratio for trapezoidal cross-sections. *Symbols* represent numerical data from (Morini et al. 2004), which have been fitted by Eq. 10

of the distributing and collecting channels and by Eq. 10 for the trapezoidal microchannels. The inlet pressure is still 10 kPa higher than the outlet pressure, and the Reynolds number are of the same order of magnitude as in Sect. 3. As in the case of rectangular cross-sections, it is observed that the relation between the optimal angle θ_T and the number n of microchannels is quasi-linear in a logarithmic scale, whatever the aspect ratio r_T^*. A similar equation

$$\theta_T = A_T\, n^{-B_T} \tag{11}$$

is then proposed to fit the calculated optimal data, with

$$A_T = -3.4553 + 497.05\, r_T^* - 202.69\, r_T^{*2} \tag{12}$$

and

$$B_T = 0.9479 - 0.0183\, r_T^* - 0.1070\, r_T^{*2}. \tag{13}$$

Figure 14 shows the values of the optimal angle θ_T as a function of the aspect ratio r_T^* for a number of microchannels ranging from 10 to 50, obtained with the analytical model (symbols) and from Eq. 11 associated with Eqs. 12–13 (lines). As in the case of rectangular microchannels, the agreement is good between the calculated optimal angle and the fitted value given by Eq. 11, with a maximal deviation less than 2.6% reached in the case of 20 microchannels with an aspect ratio $r_T^* = 0.6$.

4.1.2 Circular segment cross-section

For this kind of section, the Poiseuille number also depends only on the aspect ratio r_C^*. It has been calculated by numerical simulation with the CFD code Fluent. For that purpose, the flow was assumed laminar and incompressible and periodic boundary conditions were imposed at the inlet and outlet sections, allowing the use of only one cell in the

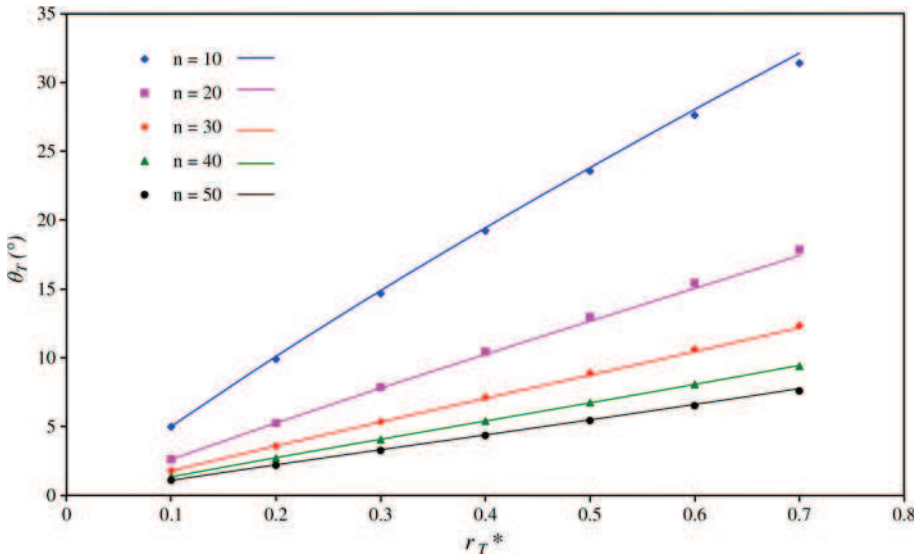

Fig. 14 Optimal angle θ_T versus aspect ratio r_T^* for various numbers n of microchannels, in the case of microchannels with trapezoidal cross-section. Values calculated by the analytical model (*symbols*) compared with data from Eq. 11 (*solid lines*)

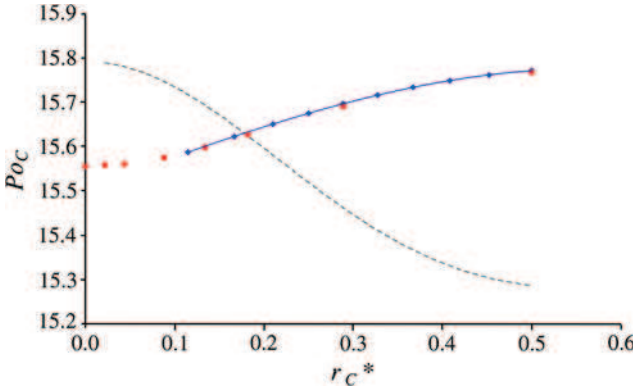

Fig. 15 Poiseuille number versus aspect ratio for circular segment cross-sections. Numerical data (*diamond symbols*) fitted by Eq. 14 (*solid line*) and compared with the numerical data from Shah and London (1978) (*circle symbols*) and the approximate model from Bahrami et al. (2007) (*dashed lines*)

streamwise direction. The influence of the mesh density has been checked, comparing the simulated Poiseuille number and the analytic value in the case of a circular cross-section. After refinement of the mesh, the numerical value was 16.0005, to be compared to the exact value, 16. The same density mesh, which corresponds to 70,000 cells in a quarter of the circular section, has been kept for all simulated circular segment sections. The corresponding Poiseuille numbers are plotted in Fig. 15 and have been fitted by the simple following equation:

$$Po_C = 15.504 + 0.72307\, r_C^* + 0.035558\, r_C^{*^2} - 0.8335\, r_C^{*^3}. \tag{14}$$

These data have been compared with data obtained by numerical simulation by Shah and London (1978) and by an approximate model by Bahrami et al. (2007). The agreement with the data from Shah and London is very good. Moreover, it is observed that the approximate model from (Bahrami et al. 2007) leads to errors of the order of 3%, which can be acceptable, but does not capture the correct increase of the Poiseuille number Po_C with the increasing aspect ratio r_C^*.

The optimal angle is deduced from the analytical solution (Eq. 5) associated with Eq. 3, in which Po is given by Eq. 2 for the rectangular channel segments of the distributing and collecting channels and by Eq. 14 for the circular segment microchannels. As in the case of rectangular and trapezoidal cross-sections, it is noticed that the relation between the optimal angle θ_C and the number n of microchannels is quasi-linear in a logarithmic scale, whatever the aspect ratio r_C^*. A similar equation

$$\theta_C = A_C\, n^{-B_C} \tag{15}$$

is then proposed to fit the data, with

$$A_C = -4.4891 + 508.57\, r_C^* - 202.31\, r_C^{*^2} \tag{16}$$

and

$$B_C = 0.9536 - 0.0120\, r_C^* - \ 0.1212\, r_C^{*^2}. \tag{17}$$

Figure 16 shows the values of the optimal angle θ_C as a function of the aspect ratio r_C^* for a number of microchannels ranging from 10 to 50, obtained with the analytical model (symbols) and from Eq. 15 associated with Eqs. 16–17 (solid lines). As in the previous cases, a good agreement is observed between the calculated optimal angle and the fitted value given by Eq. 15, with a maximal deviation of the order of 1.8% reached in the case $n = 20$ and $r_C^* = 0.5$.

In conclusion, whatever the considered cross-section of the microchannels, the optimal angle of the distributing and collecting channels for a uniform residence time distribution of the liquid in the microchannels can be accurately calculated by the following simple equation:

$$\theta = \left(A_0 + A_1\, r^* + A_2\, r^{*^2}\right) n^{-\left(B_0 + B_1\, r^* + B_2\, r^{*^2}\right)}. \tag{18}$$

The values of coefficients $(A_0, A_1, A_2, B_0, B_1, B_2)$ are summarized in Table 5 for the three kinds of cross-section.

4.2 Application to gas microflows

The analytical model for gas flow is based on the same approximation than the previous model for liquids and the study focuses on the same geometrical parameters. The hydraulic resistance, however, takes into account the compressibility of the flow as well as its rarefaction. It is assumed that the regime is the slip flow regime, which can be accurately modelled in rectangular microchannels with second-order slip boundary conditions up to Knudsen numbers of the order of 0.5 (Colin et al. 2004; Pitakarnnop et al. 2010). These values of the Knudsen number can be experienced in rather large microchannels such as those detailed in Table 1, provided the pressure is low enough, which is the case in a number of practical applications. For higher pressures, rarefaction becomes negligible, but compressibility should be taken into account, and the below model is still valid with $Kn_{out} \to 0$. Second-order boundary conditions have been proposed by Deissler (1964). In the case of a rectangular cross-section defined by $x \in [-w_c/2; +w_c/2]$ and $x \in [-d/2; +d/2]$, the slip velocity at the walls reads:

$$\begin{aligned} u|_{x=\pm\frac{w_c}{2}} &= \mp\frac{2-\sigma}{\sigma}\lambda\left.\frac{\partial u}{\partial x}\right|_{x=\pm\frac{w_c}{2}} - \frac{9}{8}\lambda^2\left(\frac{\partial^2 u}{\partial x^2} + \frac{1}{2}\frac{\partial^2 u}{\partial y^2}\right)\Bigg|_{x=\pm\frac{w_c}{2}} \\ u|_{y=\pm\frac{d}{2}} &= \mp\frac{2-\sigma}{\sigma}\lambda\left.\frac{\partial u}{\partial y}\right|_{y=\pm\frac{d}{2}} - \frac{9}{8}\lambda^2\left(\frac{\partial^2 u}{\partial y^2} + \frac{1}{2}\frac{\partial^2 u}{\partial x^2}\right)\Bigg|_{y=\pm\frac{d}{2}} \end{aligned} \tag{19}$$

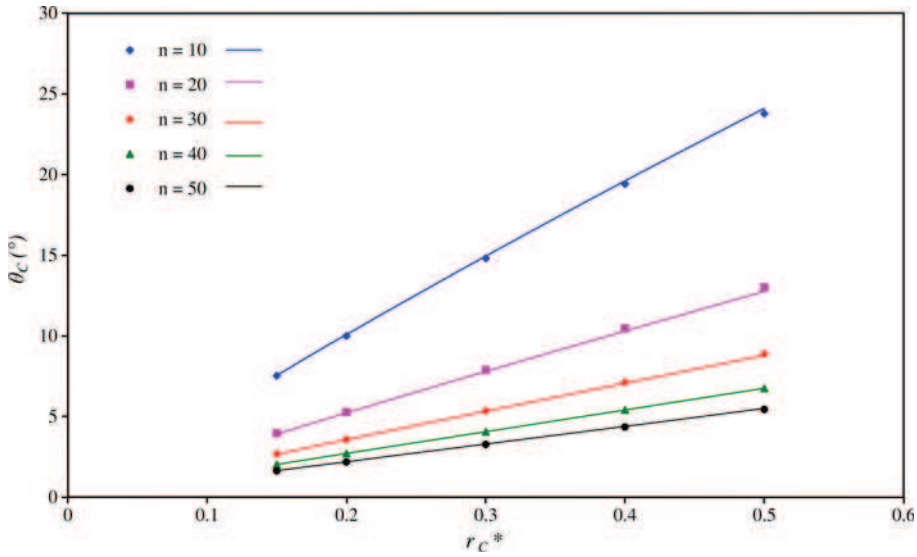

Fig. 16 Optimal angle θ_C versus aspect ratio r_C^* for various numbers n of microchannels, in the case of microchannels with circular segment cross-section. Values calculated by the analytical model (*symbols*) compared with data from Eq. 15 (*solid lines*)

Table 5 Values of coefficients used in Eq. 18 for calculating the optimal angle of distributing and collecting channels, according to the shape of the microchannels cross-sections

	A_0	A_1	A_2	B_0	B_1	B_2
Rectangular	−6.4309	575.55	−278.71	0.9801	−0.0425	−0.0888
Trapezoidal	−3.4553	497.05	−202.69	0.9479	−0.0183	−0.1070
Circular segment	−4.4891	508.57	−202.31	0.9536	−0.0120	−0.1212

In this equation, u is the streamwise velocity, λ is the mean free path of the molecules and σ is the tangential momentum accommodation coefficient. With the assumption of locally fully developed and isothermal flow, Aubert and Colin (2001) solved the compressible Navier–Stokes equations with these boundary conditions and calculated the mass flowrate

$$\dot{M} = \frac{d^4 P_{out}^2}{4 r_R^* \mu L R T}\left(\frac{a_1\left(\Pi^2-1\right)}{2} + a_2 Kn_{out}(\Pi-1) + a_3 Kn_{out}^2 \ln \Pi\right), \tag{20}$$

through a rectangular microchannel of length L with an aspect ratio r_R^*. In Eq. 20, $\Pi = P_{in}/P_{out}$ is the inlet over outlet pressure ratio, T the temperature and R the specific constant of the gas. Coefficients (a_1, a_2, a_3) depend on the accommodation coefficient σ and on the aspect ratio r_R^* (Aubert and Colin 2001; Kandlikar et al. 2006). The outlet Knudsen number

$$Kn_{out} = \frac{\lambda_{out}}{d}, \tag{21}$$

is based on the depth d of the channel and on the outlet mean free path of the molecules

$$\lambda_{out} = k_2 \frac{\mu\sqrt{RT}}{P_{out}}, \tag{22}$$

where k_2 is a constant depending on the gas studied and on the inverse power law model describing the collision of the molecules. Among the models available in the literature, one of the most accurate is the variable soft spheres model (Koura and Matsumoto 1991; Kandlikar et al. 2006), for which

$$k_2 = \frac{4\alpha(7-2\omega)(5-2\omega)}{5(\alpha+1)(\alpha+2)\sqrt{2\pi}}, \tag{23}$$

where α and ω are function of the gas species. As an example, for argon, $\alpha = 1.40$ and $\omega = 0.81$. The latter coefficient allows calculating the dynamic viscosity

$$\mu = \mu_0 \left(\frac{T}{T_0}\right)^{\omega} \tag{24}$$

at the temperature T, once the dynamic viscosity μ_0 is known at a reference temperature T_0. From Eq. 20, it is easy to obtain the hydraulic resistance in the case of gas flow as:

$$R_h = \frac{4 r_R^* \mu L R T}{P_{out} d^4}\left(\frac{a_1(\Pi+1)}{2} + a_2 Kn_{out} + a_3 Kn_{out}^2 \frac{\ln \Pi}{\Pi - 1}\right)^{-1}. \tag{25}$$

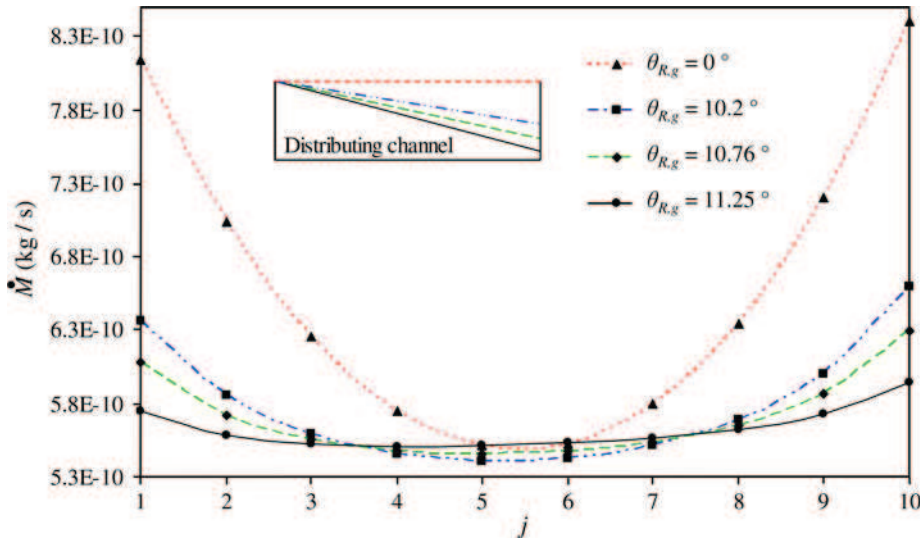

Fig. 17 Mass flowrate distribution of argon gas in a 10-microchannel reactor for the initial layout ($\theta = 0$) and the optimal layout ($\theta = 11.25°$)

It depends on the outlet and inlet pressures, which was not the case for liquid flows (see Eq. 3). With this new expression of the hydraulic resistance, the problem is still given by Eq. 5 in which **A** now depends on pressures P_j and P'_j.

The analytical optimisation is illustrated by Fig. 17, relative to the initial microreactor with rectangular microchannels detailed in Table 1 submitted to a flow of argon with an inlet pressure $P_{in} = 4.8$ kPa and an outlet pressure $P_{in} = 4.0$ kPa. The temperature $T = 298$ K is uniform and the mean Knudsen number is of the order of 10^{-1}. Due to both compressibility and rarefaction, it is no longer possible to find a perfect uniform flowrate distribution and the side microchannels always exhibit a higher flowrate than the other microchannels. The symmetry between microchannel j and microchannel $n - j$ is also lost. Nevertheless, the deviation between the flowrates in the side and central microchannels is reduced from 48% in the initial configuration to 2% in the optimised one, for an angle $\theta = 11.25°$.

5 Conclusions

A simple analytical model for optimising the residence time distribution of liquid in a multi-channel microreactor has been proposed, for different shapes of the microchannels cross-sections. The accuracy of this analytical model has been discussed from a comparison with CFD and hybrid simulations. It has been shown that a uniform flowrate distribution can be achieved with a very good precision by only modifying the angle of the tapered distributing and collecting channels. A simple equation has been proposed for rapid optimisation of the microreactor, according to the aspect ratio of the microchannel cross-section and to the number of parallel microchannels. Finally, it has been shown that the model could be extended to the case of gas flows, taking into account the effects of compressibility and rarefaction.

Based on the above optimization model, a first electrochemical microreactor composed of two platinum electrodes etched with 150 circular segment microchannels has been designed. It will be used for synthesizing probe molecules devoted to medical imaging for tumor detection. Promising preliminary results have been obtained with benchmark tests for the electrochemical synthesis of some reference molecules.

References

Aubert C, Colin S (2001) High-order boundary conditions for gaseous flows in rectangular microchannels. Microscale Thermophys Eng 5(1):41–54

Bahrami M, Michael Yovanovich M, Richard Culham J (2007) A novel solution for pressure drop in singly connected microchannels of arbitrary cross-section. Int J Heat Mass Transf 50(13–14):2492–2502

Chen Y, Cheng P (2002) Heat transfer and pressure drop in fractal tree-like microchannel nets. Int J Heat Mass Transf 45(13):2643–2648

Cho ES, Choi JW, Yoon JS, Kim MS (2010) Modeling and simulation on the mass flow distribution in microchannel heat sinks with non-uniform heat flux conditions. Int J Heat Mass Transf 53(7–8):1341

Colin S (2005) Rarefaction and compressibility effects on steady and transient gas flows in microchannels. Microfluid Nanofluid 1(3):268–279

Colin S, Lalonde P, Caen R (2004) Validation of a second-order slip flow model in rectangular microchannels. Heat Transf Eng 25(3):23–30

Commenge JM, Falk L, Corriou J-P, Matlosz M (2005) Analysis of microstructured reactor characteristics for process miniaturization and intensification. Chem Eng Technol 28(4):446–458

Commenge JM, Falk L, Corriou JP, Matlosz M (2002) Optimal design for flow uniformity in microchannel reactors. AIChE J 48(2):345–358

Deissler RG (1964) An analysis of second-order slip flow and temperature-jump boundary conditions for rarefied gases. Int J Heat Mass Transf 7:681–694

Delsman ER, Pierik A, de Croon MHJM, Kramer GJ, Schouten JC (2004) MicrochanneI plate geometry optimization for even flow distribution at high flow rates. Chem Eng Res Des 82(A2):267–273

Gravesen P, Branebjerg J, Jensen OS (1993) Microfluidics—a review. J Micromech Microeng 3(4):168–182

Jang J-Y, Cheng C-H, Huang Y-X (2010) Optimization of channel width distribution of a gas flow field by integrating computational fluid dynamics code with a simplified conjugate-gradient method. Energy Fuel 24(1):570–580

Kandlikar SG, Garimella S, Li D, Colin S, King MR (2006) Heat transfer and fluid flow in minichannels and microchannels. Elsevier, Oxford

Koura K, Matsumoto H (1991) Variable soft sphere molecular model for inverse-power-law or Lennard-Jones potential. Phys Fluids A 3(10):2459–2465

Löwe H, Ehrfeld W (1999) State of the art in microreaction technology: concepts manufacturing and applications. Electrochim Acta 44(21–22):3679–3689

Madou MJ (2002) MEMS fabrication. In: Gad-el-Hak M (ed) The MEMS Handbook. CRC Press, New York, pp 16.11–16.183

Morini GL (2004) Single-phase convective heat transfer in microchannels: a review of experimental results. Int J Therm Sci 43(7):631–651

Morini GL, Spiga M, Tartarini P (2004) The rarefaction effect on the friction factor of gas flow in microchannels. Superlattices Microstruct 35(3–6):587

Peterson RB (1999) Numerical modelling of conduction effects in microscale counterflow heat exchangers. Microscale Thermophys Eng 3(1):17–30

Pitakarnnop J, Varoutis S, Valougeorgis D, Geoffroy S, Baldas L, Colin S (2010) A novel experimental setup for gas microflows. Microfluid Nanofluid 8(1):57–72

Saber M, Commenge J-M, Falk L (2009) Rapid design of channel multi-scale networks with minimum flow maldistribution. Chem Eng Process 48(3):723–733

Saber M, Commenge JM, Falk L (2010) Microreactor numbering-up in multi-scale networks for industrial-scale applications: impact of flow maldistribution on the reactor performances. Chem Eng Sci 65:372–379

Shah RK, London AL (1978) Laminar flow forced convection in ducts. Academic Press, New York

Shoji S, Esashi M (1994) Microflow devices and systems. J Micromech Microeng 4(4):157–171

Vlachos DG (1998) Stochastic modelling of chemical microreactors with detailed kinetics - induction times and ignitions of H-2 in air. Chem Eng Sci 53(1):157–168

Ziogas A, Kolb G, O'Connell M, Attour A, Lapicque F, Matlosz M, Rode S (2009) Electrochemical microstructured reactors: design and application in organic synthesis. J Appl Electrochem 39(12):2297–2313